

Deinterlacing Network for Early Interlaced Videos

Yang Zhao, Wei Jia, Ronggang Wang, Xiaoping Liu, Xuesong Gao, Weiqiang Chen, and Wen Gao *Fellow, IEEE*

Abstract—With the rapid development of image restoration techniques, high-definition reconstruction of early videos has achieved impressive results. However, there are few studies about the interlacing artifacts that often appear in early videos and significantly affect visual perception. Traditional deinterlacing approaches are mainly focused on early interlacing scanning systems and thus cannot handle the complex and complicated artifacts in real-world early interlaced videos. Hence, this paper proposes a specific deinterlacing network (DIN), which is motivated by the traditional deinterlacing strategy. The proposed DIN consists of two stages, *i.e.*, a cooperative vertical interpolation stage for split fields, and a merging stage that is applied to perceive movements and remove ghost artifacts. Experimental results demonstrate that the proposed method can effectively remove complex artifacts in early interlaced videos.

Index Terms—deinterlacing, early videos, interlacing artifacts

I. INTRODUCTION

Interlacing artifacts are commonly observed in many early videos, which are often represented as significant comb teeth or aliasing effects, as illustrated in Fig. 1 (a). These artifacts are problems of a specific period caused by interlacing scanning in early television systems, *e.g.*, NTSC, PAL, and SECAM, in the middle and late twentieth century. The interlaced scanning mechanism of early TV systems is shown in Fig. 2. In the interlaced frame, the odd lines and even lines are scanned from two different frames, *i.e.*, the odd/top/first field and the even/bottom/second field. The two fields cannot be exactly aligned; hence, comb teeth aliasing appears in these different areas, especially when there are large movements between the two fields.

Traditional deinterlacing methods [1], [2] are mainly designed for early TV systems. However, since the interlaced mechanism is not often used currently, related studies of deinterlacing naturally become fewer. However, with the rapid development of deep learning and video processing techniques in recent years, high-definition reproductions of early videos have received considerable attention. There have been many

This work is supported by grants from the National Natural Science Foundation of China (Nos. 61972129, 61672063, 61673157), the Fundamental Research Funds for the Central Universities (No. PA2018GDQT0014), and Shenzhen Research Projects of JCYJ20180503182128089 and 201806080921419290. R. Wang is the corresponding author.

Y. Zhao, W. Jia, and X. Liu are with the School of Computers and Information, Hefei University of Technology, Hefei 230009, China (e-mail: yzhao@hfut.edu.cn; jiawei@hfut.edu.cn; lxp@hfut.edu.cn).

R. Wang, and W. Gao are with the School of Electronic and Computer Engineering, Peking University Shenzhen Graduate School, 2199 Lishui Road, Shenzhen 518055, China (e-mail: rgwang@pkusz.edu.cn; wgao@pku.edu.cn).

X. Gao, and W. Chen are with the State Key Laboratory of Digital Multimedia Technology, Hisense Co., Ltd., Qingdao, China (e-mail: gaouxuesong@tju.edu.cn, chenweiqiang@hisense.com).

Y. Zhao, R. Wang, and W. Gao are also with Peng Cheng Laboratory, Shenzhen 518000, China.

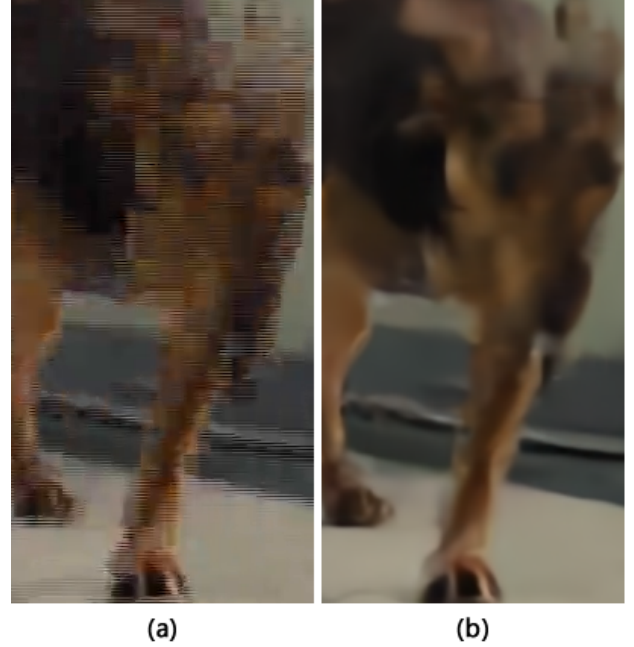


Fig. 1. An example of an interlaced frame, (a) interlaced frame, (b) deinterlaced result of the proposed method.

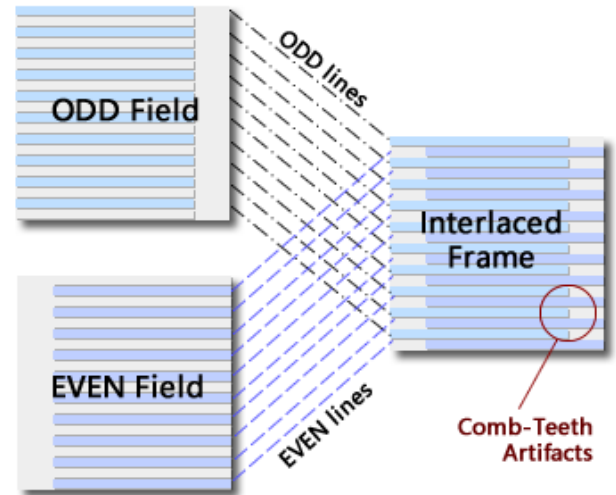


Fig. 2. Illustration of the interlaced scanning mechanism.

classical and impressive videos in the past several decades. For audiences, these early videos are related to their reminiscence or valuable childhood memories. For producers, the cost and venture of repairing a famous early video are much lower than developing a brand-new video. Unfortunately, there are various

unpleasant artifacts in early videos, of which interlacing is one of the most obvious unnatural artifacts. Recent state-of-the-art (SOTA) image restoration models cannot directly solve interlacing artifacts because interlacing is caused by specific artificial mechanism. Additionally, interlaced effects are often mixed with many other unnatural artifacts in early videos, such as blocking and noise during compression, transfer, and storage. The performances of traditional deinterlacing methods thus often significantly decrease for these complex and complicated artifacts. In summary, the motivation of this paper is to specifically design an effective deinterlacing network for the restoration of real-world early videos.

We define the traditional interlaced scanning mechanism as $\mathbf{Y} = S(\mathbf{X}_1, \mathbf{X}_2)$, where \mathbf{Y} denotes the interlaced frame, $S(\cdot)$ is the interlaced scanning function, and $\mathbf{X}_1, \mathbf{X}_2$ denote the odd and even fields. Traditional deinterlacing methods focus on the reversed process of $S(\cdot)$, which can be roughly divided into three categories, *i.e.*, temporal interpolation, spatial interpolation, and motion-based approaches. Temporal interpolation-based deinterlacing utilizes adjacent frames to interpolate the missing lines. However, the differences between two frames lead to visible artifacts when there are large movements in adjacent frames. Spatial interpolation is another kind of basic deinterlacing technique that adopts only one field to estimate the whole frame. Single field interpolation fills the missing lines by means of neighbour lines or local patches and can avoid the interlaced aliasing caused by two misaligned fields. However, the vertical interpolation is only applied to one field, and the detailed information of another field is totally omitted. The simplest spatial interpolation is the line average (LA). Since interlaced artifacts mainly appear around the edges, the edge line average (ELA) improves the LA by focusing the edge area. Because interlaced aliasing is more significant than blur of interpolation, various single field interpolation methods have been proposed in the past decades, for instance, edge detection with fuzzy logic [3], block-wise autoregression [4], bilateral filtering model [5], locality and similarity adaption [6], the maximum a posteriori (MAP) model [7] and least square methods [8]. To further refine the visual quality, visual saliency is also introduced to improve deinterlacing, for example, spectral residual visual saliency-based deinterlacing [9], [10]. There are also some single field interpolation methods for special applications, such as GPU-parallel implementation of edge-directed interpolation [11] and deinterlacing for 1080p-to-8KUHD [12]. To improve deinterlacing methods for large movements, motion-based methods have been proposed to make use of two fields [13]–[15] or adaptively improve single field methods [16], [17]. Many motion-compensation-based methods have also been introduced to calculate motion vectors between two frames to estimate the movements. Proper temporal or spatial interpolations are then applied according to the estimated movements [18]–[20].

In recent decades, many effective learning-based models have been proposed for related reconstruction tasks, such as dictionary learning [21]–[23] and sparse representation [24], [25]. Some learning-based deinterlacing algorithms have also been proposed, *e.g.*, Choi et al [26] used a joint dictionary

learning method to reconstruct interlaced high dynamic range video. In recent years, many deep neural network (DNN)-based methods have achieved superior performances than traditional methods in many low-level vision tasks [27]–[35]. Zhu et al. [36] first introduced a shallow deinterlacing convolutional neural network (DICNN) to video deinterlacing tasks and obtained impressive results. However, by focusing on deinterlacing early videos with multiple kinds of artifacts, there are still many directions to further improve this DICNN method. First, DICNN was designed for real-time applications and thus adopts a shallow super-resolution CNN (SRCNN) architecture [29]. However, the learning ability of light networks is lower than that of recent deeper models and cannot handle complicated artifacts in real-world early videos well. In this paper, the degradation process of interlaced early video can be computed as $\mathbf{Y} = C(S(\mathbf{X}_1, \mathbf{X}_2)) + \mathbf{n}$, where $C(\cdot)$ denotes the video compression process and \mathbf{n} represents noise. Hence, the proposed deinterlacing method for early video should also consider the complex interlacing artifacts mixed with other compression artifacts and noise. Second, the DICNN divides the output feature maps into two groups and then uses two convolutional layers to obtain two output frames. However, the entire input frame still contains significant comb teeth artifacts, which makes the network hard to train. Third, the forward computation of DICNN utilizes full resolution. In many recent super-resolution methods [31]–[33], features are often reconstructed in low-resolution space, and then an upsampling module is added at the end of the network. Hence, the deinterlacing network can also reduce the computational cost by using a similar strategy.

To address the interlacing and other mixed artifacts in early videos, we propose a deinterlacing network (DIN) that is designed based on the analysis of the traditional interlacing scanning mechanism. The proposed DIN consists of two stages: the co-interpolation stage and the field-merging stage. In the co-interpolation stage, the input frame is first divided into odd field and even field, and then the two fields are simultaneously inputted into a ResNet to implement vertical interpolation. Hence, the network can clearly know that these two fields are from two different frames and can still make use of the mutual latent features since these two frames have many similar contents. Additionally, the vertical pixel-shuffling module is adopted so that the former feature maps have half the size of the whole frame. In the field-merging stage, the interpolated fields are fused to the final output. The ResNet structure is selected to avoid the loss of high-frequency details. Note that larger receptive fields are needed in this stage for perceiving the movements and removing the ghost artifacts of the merged frame. Another downscale and reconstruction channel is thus added to achieve a larger receptive field. Moreover, it is difficult to obtain ground truth for early videos, and we train the proposed DIN on a synthetic dataset and test it on both the dataset and real-world early video frames.

Overall, the contributions of this paper are summarized as follows:

- 1) Traditional deinterlacing methods mainly solve the revision process of interlacing. This paper focuses on the high-

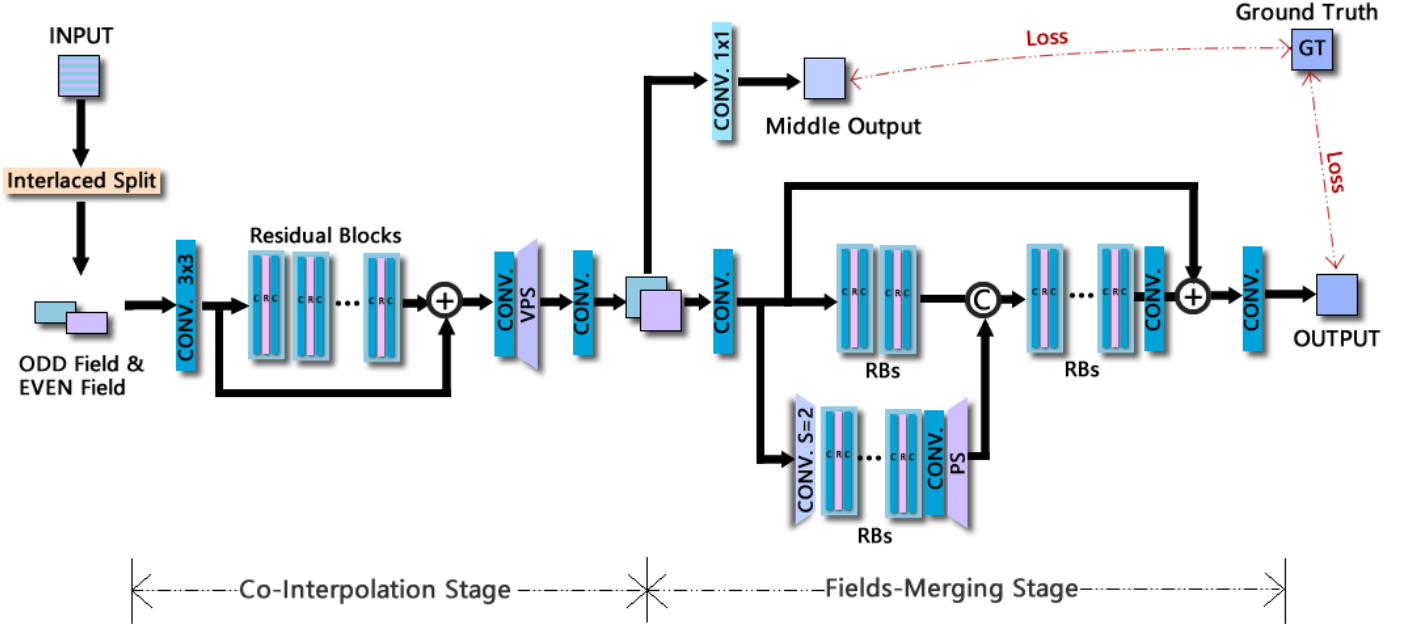


Fig. 3. Architecture of the proposed deinterlacing network.

definition restoration of early interlaced videos, which contain significant interlaced and other mixed artifacts, such as compression noise.

- 2) The architecture of DIN is specifically designed based on the analysis of the interlacing mechanism. The different odd and even fields are split and reconstructed individually so that the network can easily learn to remove interlaced artifacts.
- 3) Another field-merging stage is used to remove ghost and other merging artifacts. Two-scale ResNet is adopted to avoid loss of pixel-level spatial details, and one channel in downscale space can effectively enlarge the receptive fields to perceive movements. Overall, the proposed two-stage network is simple but naturally suitable for deinterlacing tasks.
- 4) Experimental results demonstrate that the proposed method can totally remove complex interlacing artifacts and significantly outperform other methods on difficult early interlaced videos.

The remainder of this paper is organized as follows. Section II introduces the proposed method in detail. Experimental results and related analyses are listed in Section III, and Section IV concludes the paper.

II. THE PROPOSED DEINTERLACING METHOD

A. Architecture of the Deinterlacing Network

Different from many image restoration tasks that have blind degradation models, interlaced scanning is a fixed artificial mechanism. Hence, the proposed network is designed specifically based on the interlaced scanning mechanism. Some traditional deinterlacing methods adopt single field interpolation to avoid significant artifacts of two misaligned frames. However, many high-frequency details are lost because only half of

the frames are utilized. Merging two interpolated fields can improve the details but also produces ghost artifacts. Hence, movement adaptive algorithms have been proposed to adaptively implement temporal and spatial fusion. Motivated by the traditional deinterlacing strategy, the proposed DIN consists of two stages, *i.e.*, the co-interpolation stage (CIS) and the fields-merging stage (FMS), as illustrated in Fig. 3. In the CIS, the interlaced input is naturally split into odd field and even field, and then the two fields are simultaneously reconstructed via a ResNet. In the second stage, a field-merging subnetwork is applied to further reduce ghost artifacts and other merging artifacts. To perceive movements at different scales, the FMS needs to have large receptive fields. Hence, the proposed DIN adopts multiscale ResNet to balance the preservation of pixel-level details and the magnification of receptive fields. As shown in Fig. 3, a downscale channel is added to the base ResNet to perceive larger movements, and then this higher-level information is concatenated back to the base ResNet. In the following, each stage is introduced and analysed in detail.

B. Co-Interpolation Stage

The main purpose of CIS is to compute the vertical interpolation of two fields, and its structure is illustrated in detail in Fig. 3. An effective enhanced super-resolution network (EDSR) [32], [33] is adopted as the backbone of CIS, which utilizes a typical ResNet structure [37] and carefully optimizes the residual blocks for image restoration tasks. Note that we do not use ResNet as a blackbox to train a deinterlacing network and do not first recover the interlaced frame and then apply interlacing scanning as in DICNN [36] either. In the proposed DIN, the input frame is split into even field and odd field according to the interlacing mechanism, which contain even lines and odd lines, respectively.

There are mainly two benefits of this split and co-interpolation subnetwork. First, the odd and even fields are used as input instead of the whole frame, which contains serious comb teeth artifacts. Hence, the disruption of interlacing artifacts is minimized during the training of the DIN. Second, the two adjacent frames have considerable similar spatial information. As a result, the two fields are inputted simultaneously into the network, which is helpful to recover the high-frequency pixel-level details.

Additionally, the split fields have half the size of the original frame. Motivated by the efficient pixel-shuffling (PS) module [31], which is widely adopted in current SOTA super-resolution methods [32], [38] to reduce the computational cost, the CIS also reconstructs the fields in low-resolution space and then utilizes a vertical pixel shuffle (VPS) at the end of the network to magnify the reconstructed features. The VPS process is illustrated in Fig. 4, which can be regarded as a special case of a normal PS module. By comparing Fig. 2 and Fig. 4, we can find an interesting coincidence that the VPS module is quite similar to the traditional interlacing scanning mechanism.

In our experiment, the CIS contains 6 residual blocks (RB). Each RB consists of a 3×3 convolutional layer (conv.), a rectified linear unit (ReLU) activation, another conv. 3×3 , and a local residual connection, as in [32]. The common global skip is used to improve the convergence of deep ResNet.

C. Fields-Merging Stage

The most significant artifact in the deinterlacing process is caused by the large movement between two fields. Hence, the subnetwork of the FMS tends to have a large receptive field to perceive movement information. Note that some commonly used architectures with large receptive fields, *e.g.*, UNet and autoencoder, often lead to the loss of pixelwise spatial details. Hence, the proposed FMS applies multiscale ResNet, which utilizes a base ResNet to maintain pixel-level information and then adds a downscale channel to perceive larger-scale movements. The final feature of the downscale channel is magnified via a PS module and then concatenated to the middle of the base ResNet.

By means of the two-scale structure, the proposed FMS can effectively preserve high-frequency details and extract differences at a larger scale simultaneously. As shown in Fig. 3, in our experiment, 3 RBs are used in the downscale channel; conv. 3×3 with stride 2 is utilized as the downsampling module, and the 2×2 PS module is adopted for upsampling after RBs. The base ResNet contains 5 RBs, which have 2 RBs before the concatenation of the downscale channel, and 3 RBs after the concatenation. The global skip connection is also used. In general, adding more scales can extract higher-level semantic information and perceive larger movement. However, the parameters and computational cost also increase accordingly. In our experiment, we have observed that two-scale FMS can already handle the deinterlacing task well. Hence, for keeping simplicity, only two scales are used in the proposed DIN.

At the end of this section, we discuss the differences between the architectures of DICNN and DIN. DICNN takes

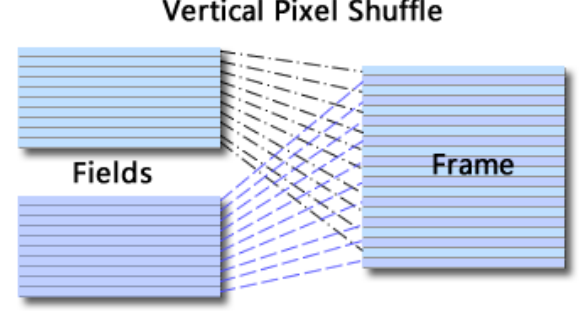


Fig. 4. Illustration of the vertical pixel shuffle module.

the whole interlaced frame as input, and then generates two reconstructed fields. The output field is combined with corresponding field in original input to form a final frame. However, the input of DIN is two split fields instead of an interlaced frame, and the output is the entire reconstructed frame. First, the DICNN is designed for deinterlacing without other degradations. For early videos with complex artifacts, combination of original low-quality field results in half of the frame being clean, but the other half still contains unnatural artifacts. Second, as mentioned earlier, splitting odd and even fields at the beginning can reduce the difficulty of the training phase. Because interlaced scanning is a manmade mechanism, we can tell this to the network instead of training a network blindly to fit this non-blind operation. In a word, the two networks are designed for different purposes. DICNN is lightweight and suitable for normal deinterlacing task, while DIN focuses on reconstruction of early videos with interlacing and other degradations.

D. Loss Function of the DIN

Similar to many image restoration models; the proposed DIN is end-to-end trained via a L_1 -distance-based loss function. As shown in Fig. 3, the two stages of the DIN are both supervised by the ground truth data so that the interpolated fields are of high quality. To constrain the two interpolated fields by means of single ground truth, a conv. 1×1 is used to linearly combine the two interpolated fields to the middle output. This supervision of intermediate output is added to directly optimize the CIS module and better train the co-interpolation stage. The entire network is then optimized by means of the following loss function:

$$L = \frac{1}{N_T} \sum_{n=1}^{N_T} [\lambda \|C_1(F_{CIS}(\mathbf{X}_1^n, \mathbf{X}_2^n)) - \mathbf{Y}^n\|_1 + (1 - \lambda) \|F_{FMS}(F_{CIS}(\mathbf{X}_1^n, \mathbf{X}_2^n)) - \mathbf{Y}^n\|_1 + p\epsilon], \quad (1)$$

where N_T denotes the total number of training samples, $\mathbf{X}_1^n, \mathbf{X}_2^n$ are the odd and even fields, \mathbf{Y}^n represents the ground truth frame, C_1 is the conv. 1×1 operation, F_{CIS} and F_{FMS} denote subnetworks of CIS and FMS, respectively, and λ is an artificial weight of the middle supervision. This weight λ is initially set as 0.5, so the CIS module can be constrained to recover better vertical interpolation results. Then, the λ is gradually reduced to 0.1 in the last half of the training phase.

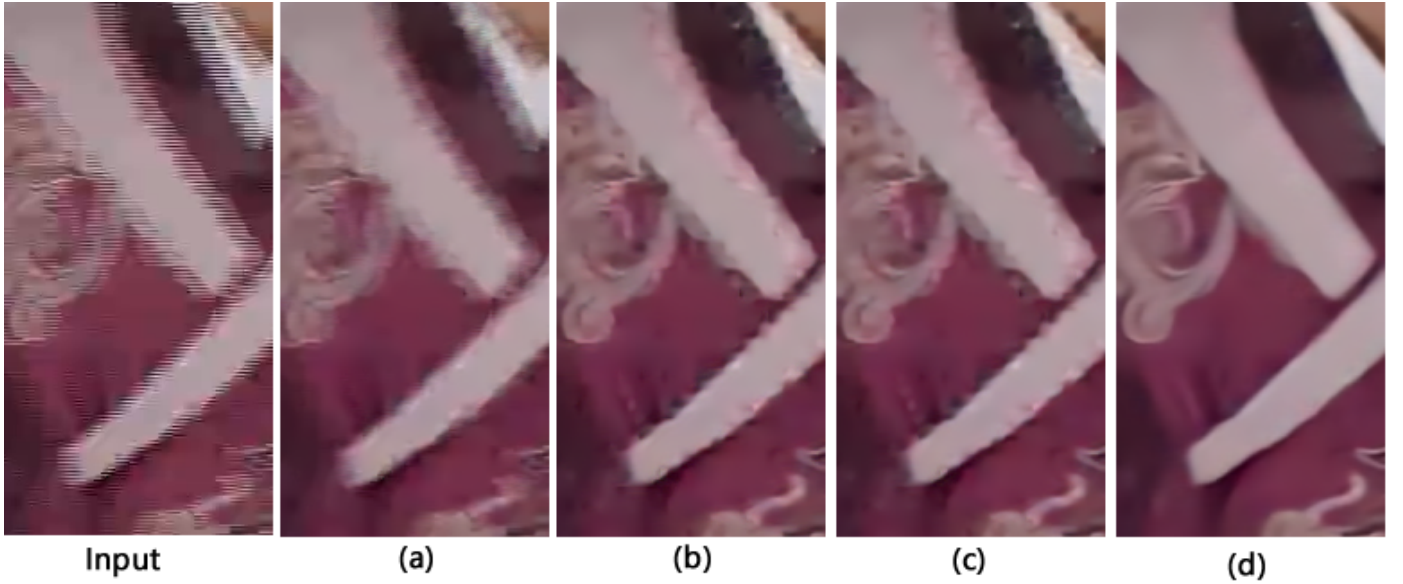


Fig. 5. Results of different methods in ablation testing, (a) CIS with entire frame as input, (b) CIS with split fields as input, (c) DIN with single-scale FMS, (d) DIN.

TABLE I
PSNR RESULTS OF DIN WITH DIFFERENT COMPONENTS ON THE
SYNTHETIC DATASET

Method	PSNR
CIS (input entire frame)	32.15
CIS (input split fields)	33.05
DIN (CIS + single-scale FMS)	33.21
DIN (CIS + FMS)	34.85
DIN (without middle supervision)	34.20
DIN (loss without disruption term)	34.79

Note that the DIN is trained on a synthetic dataset and often converges very fast in the first several epochs. Hence, we introduce a random disruption term $p\varepsilon$ in this loss function to slow the convergence of the trained network. In this paper, p is a random number from -1 to 1 , and ε is experimentally set as 10^{-5} .

E. Implementational Details

In our experiment, a total of 100,000 training patch pairs with a size of 256×256 are selected from the training set, and then these patches are augmented via horizontal and vertical flipping. It should be noted that rotation cannot be used for data augmentation in deinterlacing because the interlaced artifacts are along the horizontal direction. In this paper, each conv. layer in RBs outputs 64 feature maps except for the last 3 RBs in FMS, which have 128 channels after the concat operation. The batch size is 16, the weights are initialized via Xavier, and the network is optimized via Adam. The initial learning rate is 10^{-4} and then decreases by a factor of 10 after every 20 epochs. This network was trained 100 epochs with a GTX1080Ti GPU by means of the MXNET platform.

To verify the effectiveness of these components of the DIN, we first compare the direct reconstruction of the entire

interlaced frame and the proposed split and co-interpolation strategy. By comparing the results in Figs. 5 (a) and (b), it can be found that directly using ResNet as a blackbox can reduce comb teeth artifacts, but it cannot remove severe interlacing. The proposed co-interpolation of two fields can reproduce much better results than directly recover the entire frame. Related PSNR values are listed in Table I. The split and co-interpolation strategy obtains a much higher PSNR than directly reconstructing the entire frame.

Note that there are still many artifacts and noises in Fig. 5 (b); hence, the FMS is applied to further remove the ghost artifacts and other noise. By comparing the PSNR results, CIS combined with single-scale FMS can increase the PSNR values. However, by comparing Figs. 5 (b) and (c), single-scale FMS cannot effectively remove these unnatural artifacts during reconstruction. As illustrated in Fig. 5 (d), the proposed DIN with multiscale FMS significantly improves the visual quality. Meanwhile, as shown in Table I, the proposed DIN can achieve much higher results by combining these effective strategies.

Moreover, the performances of DIN without supervised middle output and DIN with normal L_1 loss are also listed in Table I. These simple tricks are also helpful for the proposed two-stage network.

III. EXPERIMENTS

A. Training and Testing Datasets

It is difficult to obtain high-quality ground truth data for real-world early videos. Hence, we generate a synthetic dataset to train the proposed DIN. Then, the trained network is not only tested on this synthetic dataset but also verified on several real-world early videos.

For training, a total of 400 video sequences are collected from the YOUKU 2K video dataset [39]. Each video sequence consists of 100 frames with 2K resolution. Note that the

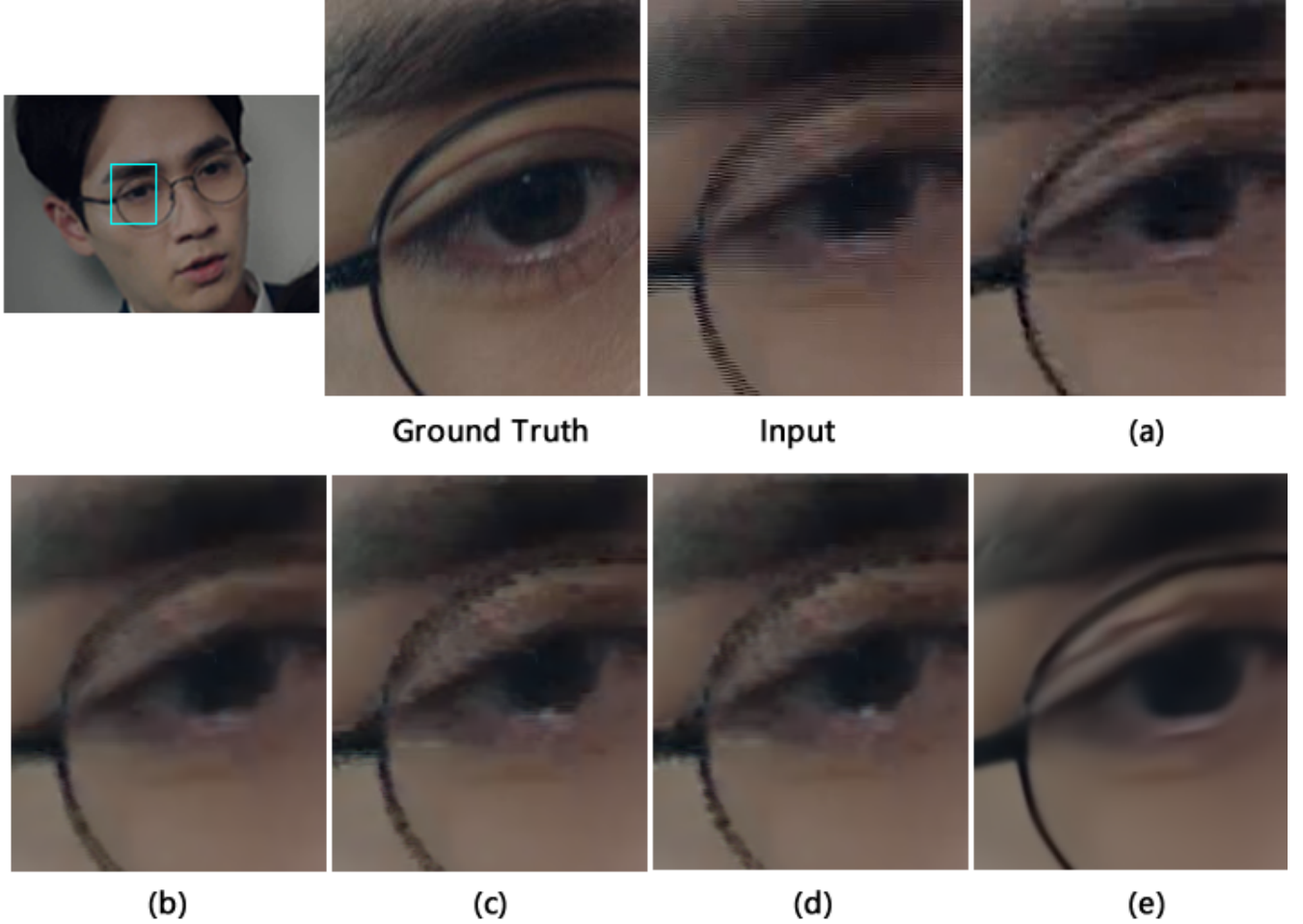


Fig. 6. Deinterlacing results of different methods, (a) single field EDSR [32], (b) retrained EDSR [32], (c) retrained SRCNN [29], (d) DICNN [36], (e) the proposed DIN.

TABLE II
PSNR AND SSIM RESULTS OF DIFFERENT DEINTERLACING METHODS ON
THE SYNTHETIC DATASET

	PSNR	SSIM	Number of Parameters
Input	30.33	0.8777	-
Single Field EDSR [32]	32.04	0.9088	5.905M
EDSR (retrain) [32]	32.65	0.9130	5.905M
SRCNN (retrain) [29]	32.43	0.9111	0.036M
DICNN [36]	32.53	0.9125	0.118M
DIN	35.17	0.9348	1.816M

cartoon sequences are not selected in this experiment. Then, the interlaced frame is produced according to the traditional interlaced scanning system, *i.e.*, the odd and even lines are scanned from two adjacent frames. The real first frame is utilized as ground truth data. Furthermore, the interlaced video is then compressed via the H.264 codec with a random “-crf” parameter from 30 to 38 by means of FFMPEG tool. This compression process is adopted to roughly simulate the mixed compression artifacts in early videos.

For testing, two image sets are used, *i.e.*, the synthetic dataset and the real-world early video dataset. In the synthetic

testing set, 40 testing frames are generated in the same way as in the training stage. In a real-world dataset, 38 interlaced frames are randomly selected from several real-world early videos to verify the generalization of the proposed method. Note that the real-world testing set does not have ground truth, and thus, the objective assessment is only applied to the synthetic dataset.

B. Experimental Results on the Synthetic Testing Set

In our experiment, the proposed DIN¹ is compared with several DNN-based methods, *e.g.*, SRCNN retrained for deinterlacing [29] and DICNN [36]. Note that DICNN is a very light network for real-time deinterlacing without severe noise; it is not designed to handle complicated noise in early videos due to few parameters. Hence, we retrain another effective deeper model EDSR [32] with 20 RBs for deinterlacing. For a fair comparison, these networks are all retrained with the same training set. In addition, traditional EDSR trained for

¹Demo videos, demo codes of the proposed DIN and its lightweight version can be obtained from the following link: <https://gitee.com/gityzhao/din/>

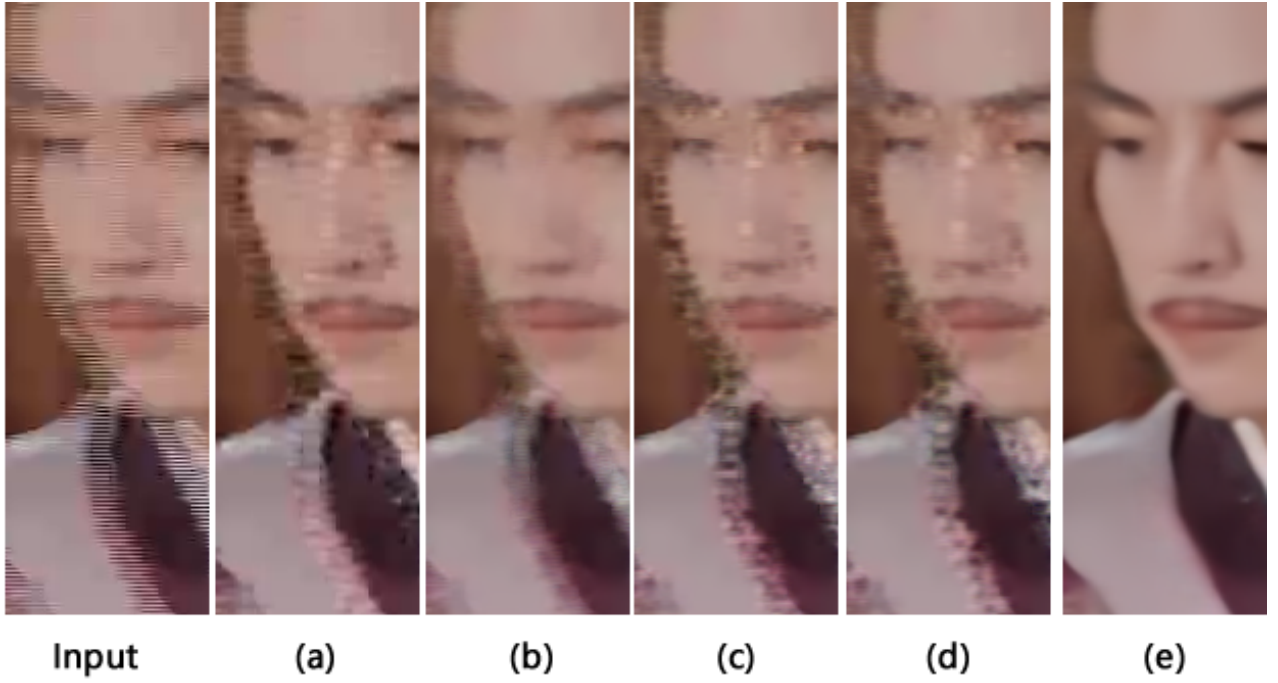


Fig. 7. Results of different methods on a severely interlaced area: (a) single field EDSR [32], (b) retrained EDSR [32], (c) retrained SRCNN [29], (d) DICNN [36], (e) the proposed DIN.

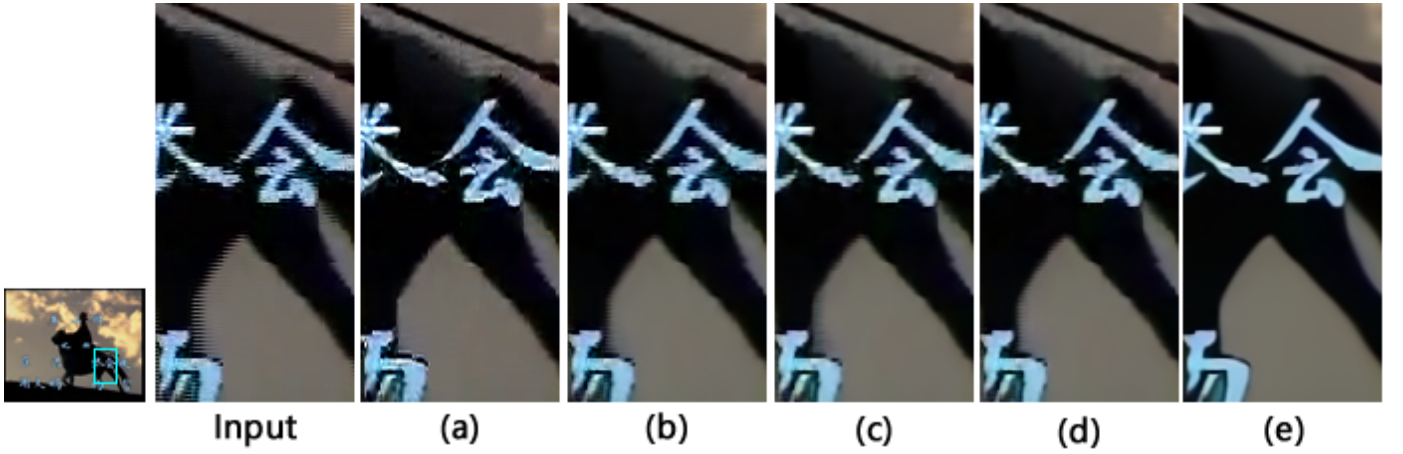


Fig. 8. Reconstruction frames of Journey to the West (1986) with different methods: (a) single field EDSR [32], (b) retrained EDSR [32], (c) retrained SRCNN [29], (d) DICNN [36], (e) the proposed DIN.

super-resolution tasks, which can be introduced as a single field interpolation deinterlacing, is also used for comparison.

Fig. 6 illustrates several reconstructed results of different methods on an interlaced and compressed frame. Several observations can be obtained from Fig. 6. First, for these complex artifacts caused by interlacing and compression, the single field EDSR can avoid comb teeth effects but also magnify many unnatural artifacts. Second, the retrained SRCNN, EDSR and DICNN can reduce interlaced aliasing, but these methods cannot totally remove mixed compression noise by directly throwing frames with mixed artifacts to the networks. Note that the EDSR performs slightly better

than SRCNN and DICNN because the EDSR is much deeper than these lightweight networks. Third, the proposed DIN can simultaneously remove interlacing and compression artifacts.

Fig. 7 is focused on the results on a frame with severe interlacing mixed with compression noise. These SOTA methods may fail to recover fine results for these difficult cases. Owing to the specifically designed deinterlacing architecture, the proposed DIN can still reproduce high visual quality results.

Related objective assessments of different methods are listed in Table II. The proposed DIN significantly outperforms other methods on the synthetic testing set, which contains various frames with mixed interlacing and compression artifacts.

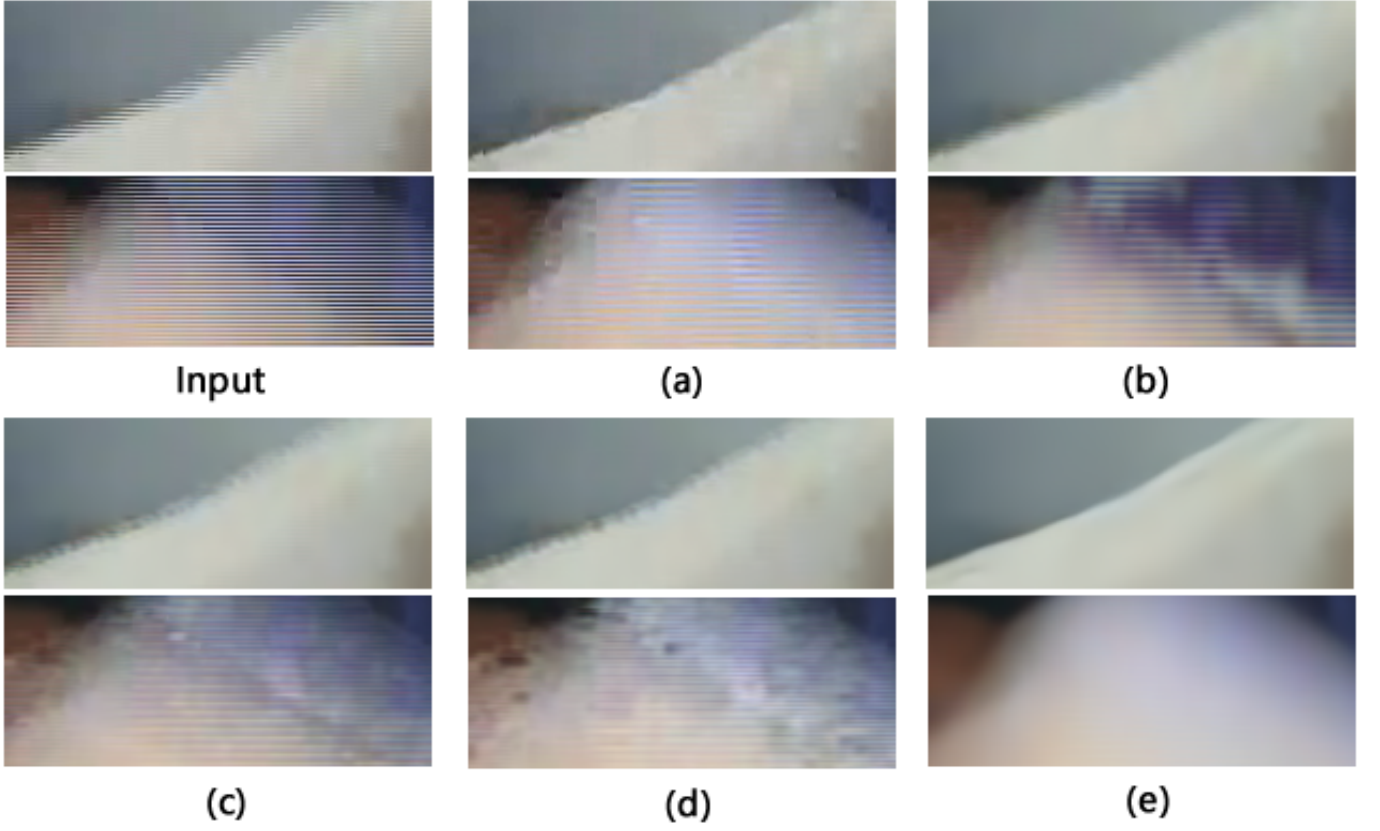


Fig. 9. Reconstruction results of two frames with different degrees of motion: (a) single field EDSR [32], (b) retrained EDSR [32], (c) retrained SRCNN [29], (d) DICNN [36], (e) the proposed DIN.

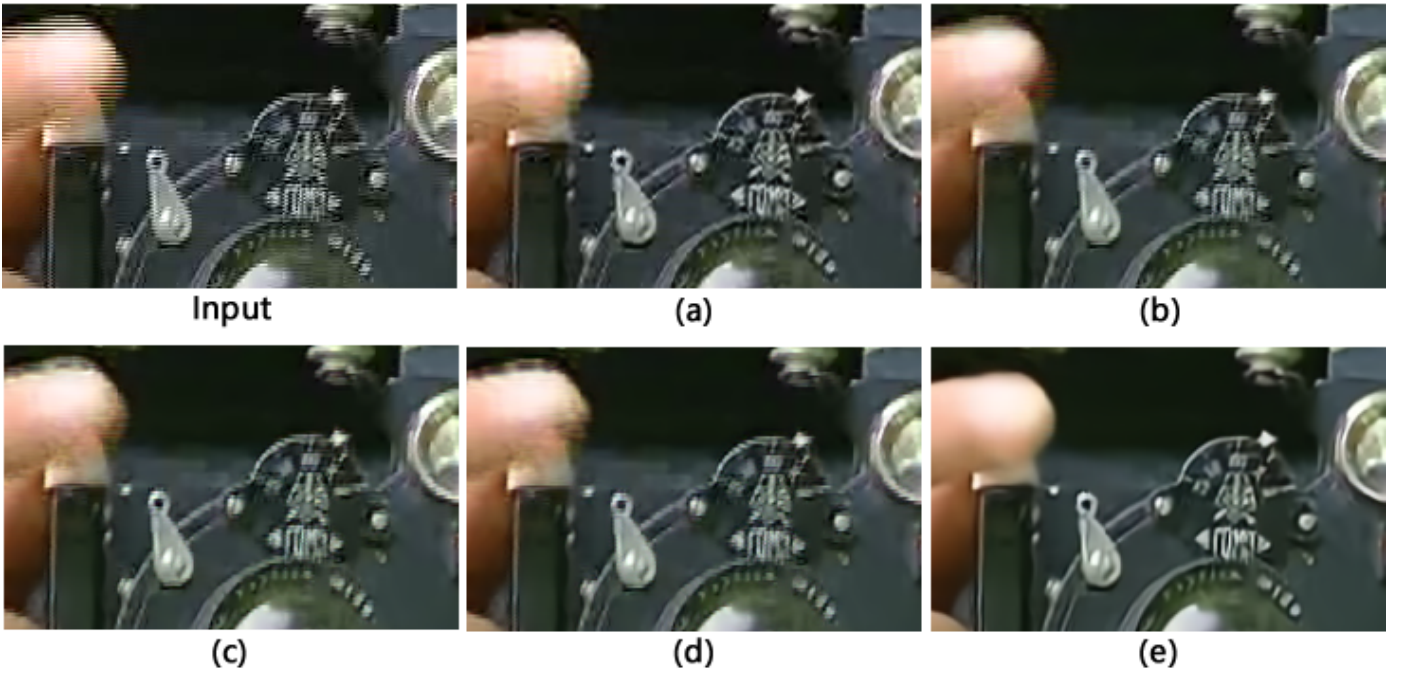


Fig. 10. Reconstruction results of real-world early videos, (a) single field EDSR [32], (b) retrained EDSR [32], (c) retrained SRCNN [29], (d) DICNN [36], (e) the proposed DIN.

Although these compared SOTA methods can perform well in deinterlacing alone, they still cannot handle the compli-

cated interlaced effects combined with significant compression noises well. Note that the DICNN is designed for real-time

deinterlacing task, which is very lightweight based on shallow SRCNN. The proposed DIN can improve the capability by means of more learnable parameters. By comparing with directly applying deeper model of EDSR, the DIN is more suitable for deinterlacing task.

C. Experimental Results on Real-World Early Videos

The main purpose of this paper is to improve the visual quality of early videos that contain severe interlacing artifacts. Hence, the proposed method is also verified on several real-world early videos in addition to the synthetic dataset.

Fig. 8 lists the reconstructed results of a frame from an early Chinese TV show “*Journey to the West (1986)*” with different methods. There is considerable aliasing, comb teeth, and compression noise in the input frame. The single field EDSR avoids comb teeth but also magnifies aliasing during vertical interpolation. The DNN methods of EDSR, SRCNN, and DICNN can reduce slight aliasing but leave ghost shadows around the severe interlacing area. In addition, these methods cannot handle noise mixed with interlacing. Note that although these methods are trained on the same dataset, the proposed DIN significantly outperforms other methods, which demonstrates that the proposed DIN is effective for these early interlaced and compressed videos.

Fig. 9 illustrates some reconstructed details of two frames with different degrees of movement. Generally speaking, larger movement usually leads to more obvious interlacing artifacts. Some findings can be obtained from Fig. 9. First, the single field EDSR tends to magnify the artifacts along the vertical direction. Second, the EDSR, SRCNN and DICNN can reduce interlacing but produce unnatural artifacts. The EDSR can recover better edges than the SRCNN and DICNN by means of a much deeper network. Third, these comparison methods fail to reproduce clean and natural results by comparing the reconstructed areas with larger motion and severe interlacing. Finally, the proposed DIN can recover clear and sharp edges without interlaced aliasing and unnatural artifacts. More deinterlaced frames on another early video are shown in Fig. 10. Some similar findings can be observed. The proposed DIN still reproduces visually better results than other methods.

The ground truth data of real-world early videos are difficult to obtain. Single stimulus subjective testing has thus been applied to compare the visual quality of reconstructed early videos. The details of the viewing conditions and test session are set according to Rec. ITU-R BT.500 [40]. A total of 15 observers are invited to score the impairment scales of six sets of frames to 5 levels, where the impairment levels 5, 4, 3, 2, and 1 denote “imperceptible impairment”, “perceptible impairment”, “slightly annoying impairment”, “annoying impairment”, and “very annoying impairment”, respectively. The average impairment scale scores are listed in Table III. It can be easily found that the proposed method achieves much higher subjective scores than other methods on real-world early videos.

At last, the shortcomings of this method are analyzed and the future work is introduced. Although DIN can effectively remove interlacing artifacts in early videos, it is based on a

TABLE III
AVERAGE IMPAIRMENT SCALE SCORES OF DIFFERENT METHODS ON REAL-WORLD EARLY VIDEOS.

	Impairment Scale Score
Input	2.14
Single Field EDSR [32]	2.50
EDSR (retrain) [32]	2.85
SRCNN (retrain) [29]	2.40
DICNN [36]	2.54
DIN	4.33

single frame. Generally speaking, the multi-frame methods can produce better temporal consistency than single-frame strategy. Therefore, in our future work, we tend to explore multi-frame versions of DIN to further improve the performance.

IV. CONCLUSION

This paper proposes a deinterlacing network (DIN) for early videos that contains interlacing and compression artifacts. The two-stage architecture of the proposed DIN is motivated by the interlacing scanning system and traditional deinterlacing strategies. The co-interpolation stage splits the interlaced frame into odd and even fields and then simultaneously estimates the vertical interpolation of two fields. Another field-merging stage is then applied to further remove ghost and other unnatural artifacts. Experimental results demonstrate that the proposed method can effectively recover high-quality results from interlaced and compressed frames. Furthermore, the proposed method also achieved impressive performance on real-world early videos that contain severe and complex interlacing artifacts.

REFERENCES

- [1] D. Gerard, and E. Bellers, “Deinterlacing-an overview,” *Proc. IEEE*, vol. 86, no.9, pp.1839-1857, 1998.
- [2] T. Doyle, “Interlaced to sequential conversion for EDTV applications,” in *Proc. International Workshop on Signal Processing of HDTV*, 1990, pp. 412-430.
- [3] P. Brox, I. Baturone, S. Solano, and J. Rios, “Edge-adaptive spatial video de-interlacing algorithms based on fuzzy logic,” *IEEE Trans. Consumer Electronics*, vol. 60, no. 3, pp.375-383, 2014.
- [4] J. Wang, G. Jeon, J. Jeong, “A block-wise autoregression-based deinterlacing algorithm,” *Journal of Display Technology*, vol.10, no.5, pp.414-419, 2013.
- [5] V. Jakhetiya, O. C. Au, S. Jaiswal, L. Jia, H. Zhang, “Fast and efficient intra-frame deinterlacing using observation model based bilateral filter,” *IEEE Int. Conf. Acoustics, Speech and Signal Process.*, 2014, pp. 5819-5823.
- [6] J. Wang, J. Gwanggil, and J. Jechang, “Efficient adaptive deinterlacing algorithm with awareness of closeness and similarity,” *Optical Engineering*, vol.51, no.1, 017003-1, 2012.
- [7] J. Wang, J. Gwanggil, and J. Jechang, “De-Interlacing algorithm using weighted least squares,” *IEEE Trans. Circuits and Syst. Video Technol.*, vol.24, no.1, pp.39-48, 2014.
- [8] J. Wang, J. Gwanggil, and J. Jechang, “Moving least-squares method for interlaced to progressive scanning format conversion,” *IEEE Trans. Circuits and Syst. Video Technol.*, vol.23, no.11, pp.1865-1872, 2013.
- [9] U. Aggarwal, M. Trocan, F. Coudoux, “Spectral saliency-based video deinterlacing,” *International Conference on Computational Collective Intelligence*, 2016, pp. 590-598.
- [10] U. Aggarwal, M. Trocan, F. Coudoux, “An HVS-inspired video deinterlacer based on visual saliency,” *Vietnam Journal of Computer Science*, vol. 4, no.1, pp.61-69, 2017.
- [11] J. Wu, Z. Song, G. Jeon, “GPU-parallel implementation of the edge-directed adaptive intra-field deinterlacing method,” *Journal of Display Technology*, vol.10, no.9, pp.746-753, 2014.

- [12] Y. Chang and C. Fan, "Spatial-domain edge-directed interpolation based de-interlacing to up-scaling technology for 1080i full HD to progressive 8K ultra HD," *IEEE Int. Conf. Consumer Electronics-Taiwan*, 2017, pp. 275-276.
- [13] D. Wang, A. Vincent, and P. Blanchfield, "Hybrid de-interlacing algorithm based on motion vector," *IEEE Trans. Circuits and Syst. Video Technol.*, vol. 15, no. 8, pp. 1019-1025, Aug. 2005.
- [14] D. Hargreaves and J. Vaisey, "Bayesian motion estimation and interpolation in the interlaced video sequences," *IEEE Trans. Image Process.*, vol. 6, no. 5, pp. 764-769, May 1997.
- [15] P. Brox, I. Baturone, and S. Sanchez-Solano, "Fuzzy motion-adaptive interpolation with picture repetition detection for deinterlacing," *IEEE Trans. Instrum. Meas.*, vol. 58, no. 9, pp. 2952-2958, Sep. 2009.
- [16] K. Lee and C. Lee, "High quality spatially registered vertical temporal filtering for deinterlacing," *IEEE Trans. Consumer Electronics*, vol. 59, no. 1, pp. 182-190, 2013.
- [17] X. Zhang and D. Wang, D., "An efficient motion adaptive deinterlacing algorithm using improved edge-based line average interpolation," *IEEE Int. Conf. Signal Process.*, 2016, pp. 659-662.
- [18] H. M. Mohammadi, Y. Savaria, and J. M. P. Langlois, "Enhanced motion compensated deinterlacing algorithm," *IET Image Process.*, vol. 6, no. 8, pp. 1041-1048, Nov. 2012.
- [19] G. Jeon, J. You, and J. Jeong, "Weighted fuzzy reasoning scheme for interlaced to progressive conversion," *IEEE Trans. Circuits and Syst. Video Technol.*, vol. 19, no. 6, pp. 842-855, 2009.
- [20] X. Zhu, Q. Huang, F. Ye, F. Liu, S. Xu, Y. Wang, Y., "Motion-compensated deinterlacing based on scene change detection," *Pacific Rim Conference on Multimedia*, Cham, 2017, pp. 397-406.
- [21] H. Chang, D. Y. Yeung, and Y. Xiong, "Super-resolution through neighbor embedding," in *Proc. IEEE Conf. Comput. Vis. Pattern Recognit.*, Jun. 2004, vol. 1, pp. 275-282.
- [22] R. Timofte, V. D. Smet, and L. V. Gool, "Anchored neighborhood regression for fast example-based super-resolution," in *Proc. IEEE Int. Conf. Comput. Vis.*, Dec. 2013, pp. 1920-1927.
- [23] Y. Zhao, R. Wang, W. Wang, W. Gao, "Multilevel modified finite radon transform network for image upsampling," *IEEE Trans. Circuits and Syst. Video Technol.*, vol. 26, no. 12, pp. 2189-2199, 2015.
- [24] J. Yang, J. Wright, T. S. Huang, "Image super-resolution via sparse representation," *IEEE Trans. Image Process.*, vol. 19, no. 11, pp. 2861-2873, 2010.
- [25] C. Jung, L. Jiao, H. Qi, and T. Sun, "Image deblocking via sparse representation," *Signal Process. Image Comm.*, vol. 27, no. 6, pp. 663-677, 2012.
- [26] I. Choi, S. Baek, M. Kim, "Reconstructing interlaced high-dynamic-range video using joint learning," *IEEE Trans. Image Process.*, vol. 26, no. 11, pp. 5353-5366, 2017.
- [27] K. Zhang, W. Zuo, Y. Chen, D. Meng, L. Zhang, L., "Beyond a gaussian denoiser: Residual learning of deep cnn for image denoising," *IEEE Trans. Image Process.*, vol. 26, no. 7, pp. 3142-3155, 2017.
- [28] C. Dong, Y. Deng, C. Change Loy, "Compression artifacts reduction by a deep convolutional network," in *Proc. IEEE Int. Conf. Comput. Vis.*, 2015, pp. 576-584.
- [29] C. Dong, C. Loy, K. He, and X. Tang, "Image super-resolution using deep convolutional networks," *IEEE Trans. Pattern Anal. Mach. Intell.*, vol. 38, no. 2, pp. 295-307, Jul. 2016.
- [30] J. Kim, J. Lee, and K. Lee, "Accurate image super-resolution using very deep convolutional networks," in *Proc. IEEE Conf. Comput. Vis. Pattern Recognit.*, Jun. 2016, vol. 1, pp. 1646-1654.
- [31] W. Shi, J. Caballer, F. Huszar, et al., "Real-Time single image and video super-resolution using an efficient sub-pixel convolutional neural network," in *Proc. IEEE Conf. Comput. Vis. Pattern Recognit.*, Jun. 2016, vol. 1, pp. 1874-1883.
- [32] B. Lim, S. Son, H. Kim, S. Nah, and K. M. Le, "Enhanced deep residual networks for single image super-resolution," in *Proc. IEEE Conf. Comput. Vis. Pattern Recognit. Workshops*, Jul. 2017, pp. 1132-1140.
- [33] R. Timofte, E. Agustsson, "Ntire 2017 challenge on single image super-resolution: Methods and results," in *Proc. IEEE Conf. Comput. Vis. Pattern Recognit. Workshops*, Jul. 2017, vol. 1, pp. 1110-1121.
- [34] Y. Zhao, R. Wang, W. Jia, W. Zuo, X. Liu, W. Gao, "Deep reconstruction of least significant bits for bit-depth expansion," *IEEE Trans. Image Process.*, vol. 28, no. 6, pp. 2847-2859, 2019.
- [35] Y. Zhao, R. Wang, Y. Chen, W. Jia, X. Liu, W. Gao, "Lighter but efficient bit-depth expansion network," *IEEE Trans. Circuits and Syst. Video Technol.*, DOI:10.1109/TCSVT.2020.2982505, 2020.
- [36] H. Zhu, X. Liu, X. Mao, T. Wong, "Real-time deep video deinterlacing," *arXiv preprint*, arXiv:1708.00187, 2017.
- [37] C. Ledig, L. Theis, F. Huszar, "Photo-realistic single image super-resolution using a generative adversarial network," *arXiv preprint*, arXiv:1609.04802, 2016.
- [38] Y. Zhang, K. Li, K. Li, L. Wang, B. Zhong, and Y. Fu, "Image super-resolution using very deep residual channel attention networks," in *Proc. Euro. Conf. Comput. Vis.*, Sept. 2018.
- [39] Youku Video Super-Resolution and Enhancement Challenge (Youku-VSRE2019) dataset, 2019. [Online]. Available: <https://tianchi.aliyun.com/dataset/dataDetail?dataId=39568>
- [40] Methodologies for the subjective assessment of the quality of television images, Rec. ITU-R BT.500, 2019. [Online]. Available: <https://www.itu.int/rec/R-REC-BT.500/en>